

Numerical simulations of two-dimensional flows around a Savonius rotor with various curvature of the blade

Yuka Yoshida, Tetuya Kawamura

(Received July 30, 2012)

Abstract

Numerical simulations of two-dimensional flows around a Savonius rotor with various curvature of the blade are investigated. The governing equations are the incompressible Navier-Stokes equations. A rotating coordinate system, that rotates at the same speed of the rotor, is used in order to simplify the boundary conditions on the blades of the rotor. Boundary fitted coordinate systems are employed to express the shape of the blades precisely. The fractional step method is used for solving basic equations. The shape of the blade is a part of ellipse. The shape of the blade is defined by changing one axis of the ellipse to investigate the effect of the blade shape on the performance of the rotor. As the result of the calculations, the relations of the blade shape and the power coefficient was found.

1. Introduction

The use of a renewable energy is one of the important issues to solve the energy shortage and to contribute the environmental protection. A wind turbine can produce the renewable energies by the wind. This wind turbine system has several features such as low power generation cost, the relatively easy introduction of equipment, and working all day without depending on the sunshine. Actually, the number of the wind turbine is increasing year by year all over the world.

A propeller shape of a horizontal type wind turbine has been chosen by the electric power industry because of its high power efficiency. On the other hand, a vertical type wind turbine, especially Savonius rotor type wind turbine, can be running without any direction control system and any starting support system, so this type is suitable for using in small scale or for a simple generator for domestic use.

Savonius rotor was designed as the vertical axis wind turbine in 1931 by S.J.Savonius.^[1] Recently, Savonius rotor is expected to be used as an emergency power supplier for its easy operation.

Previous studies on Savonius rotor are carried out to optimize the designing of the blades for acquiring the high power efficiency. Ushiyama et al.^[2] studied the variables of aspect ratio, overlap ratio and separation gap of two buckets. Fujisawa^[3] and Ishimatsu et al.^[4] investigated overlap ratios. Kuwana et al.^[5] and Kamoji^[6] proposed

the twisted blade shape Savonius rotor to improve the problem of large torque variation. Sato et al.^[7] studied S-shaped rotor with varying the blade curvature and separation gap.

In this study, the effect of the curvature of the blade is continued to examine.

2. Preparation of the calculation

2.1 Blade shapes of the Savonius rotor

The schematic of Savonius rotor is shown in Figure 1.

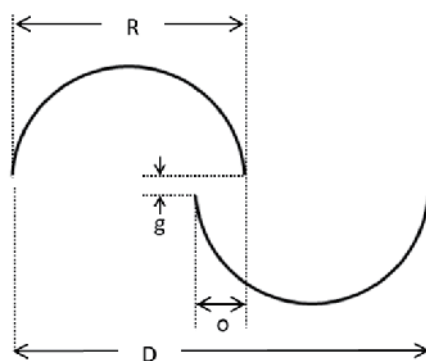


Fig. 1 The schematic of Savonius rotor

R:Bucket chord

D:Rotor diameter

OL:Overlap (o/R)

SG:Separation gap (g/R)

λ :Tip speed ratio

In this study, three shapes of the Savonius rotors blades are compared. The curvature of the blade is defined by the equation of an ellipse(Eq.1).

$$\frac{x^2}{a^2} + \frac{y^2}{b^2} = 1 \quad \text{Eq. 1}$$

The parameter **a** is fixed at 1.00 and the parameter **b** is variable. If **b** is equal to 1.00, the shape of the blade is semicircular and the conventional shape of Savonius rotor. Figure 2 shows the blade shapes which are calculated in this study. The conventional shape($b=1.00$) and other two shapes($b=0.75,1.25$) are calculated.

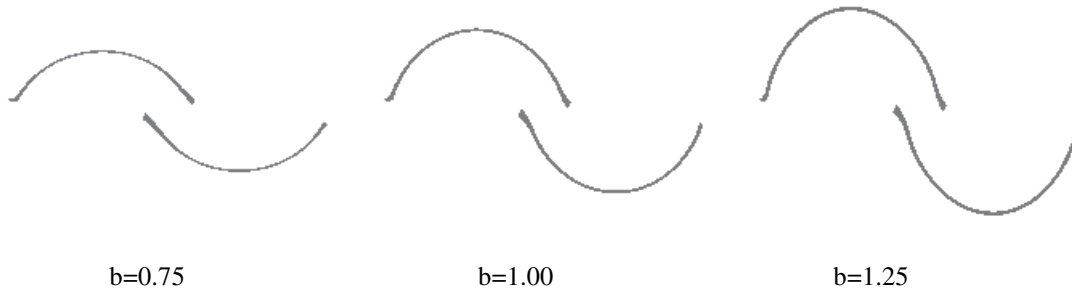


Fig. 2 The blade shapes of the rotor

Ushiyama et.al. reported the overlap ratio(o/D) of 0.20-0.30 and no separation gap(g/D) give the best performance^[2]. The overlap ratio and the separation gap are fixed to 0.28 and zero respectively in this study.

2.2 Numerical method

The governing equations are given by the two-dimensional incompressible form of the Navier-Stokes equations and continuity equations described below.

$$\frac{d\mathbf{v}}{dt} + (\mathbf{v} \cdot \nabla)\mathbf{v} = \frac{1}{Re} \nabla^2 \mathbf{v} - \nabla \mathbf{p} \quad \text{Eq. 2}$$

$$\nabla \cdot \mathbf{v} = 0 \quad \text{Eq. 3}$$

These equations are expressed in the stationary coordinate system.

The rotational coordinate system which rotate at the same angular velocity with the turbine are used to calculate. Equations are expressed in the rotational coordinate system which are as follows.

$$\mathbf{X} = \mathbf{x} \cos \theta - \mathbf{y} \sin \theta \quad \text{Eq. 4}$$

$$\mathbf{Y} = \mathbf{x} \sin \theta + \mathbf{y} \cos \theta \quad \text{Eq. 5}$$

$$\mathbf{U} = \mathbf{u} \cos \theta - \mathbf{v} \sin \theta - \omega \mathbf{Y} \quad \text{Eq. 6}$$

$$\mathbf{V} = \mathbf{u} \sin \theta + \mathbf{v} \cos \theta + \omega \mathbf{X} \quad \text{Eq. 7}$$

$$\frac{\partial \mathbf{U}}{\partial t} + \mathbf{U} \frac{\partial \mathbf{U}}{\partial \mathbf{X}} + \mathbf{V} \frac{\partial \mathbf{U}}{\partial \mathbf{Y}} - \omega^2 \mathbf{X} + 2\omega \mathbf{V} = -\frac{\partial \mathbf{p}}{\partial \mathbf{X}} + \frac{1}{Re} \left(\frac{\partial^2 \mathbf{U}}{\partial \mathbf{X}^2} + \frac{\partial^2 \mathbf{U}}{\partial \mathbf{Y}^2} \right) \quad \text{Eq. 8}$$

$$\frac{\partial \mathbf{V}}{\partial t} + \mathbf{U} \frac{\partial \mathbf{V}}{\partial \mathbf{X}} + \mathbf{V} \frac{\partial \mathbf{V}}{\partial \mathbf{Y}} - \omega^2 \mathbf{Y} - 2\omega \mathbf{U} = -\frac{\partial \mathbf{p}}{\partial \mathbf{Y}} + \frac{1}{Re} \left(\frac{\partial^2 \mathbf{V}}{\partial \mathbf{X}^2} + \frac{\partial^2 \mathbf{V}}{\partial \mathbf{Y}^2} \right) \quad \text{Eq. 9}$$

$$\frac{\partial \mathbf{U}}{\partial \mathbf{X}} + \frac{\partial \mathbf{V}}{\partial \mathbf{Y}} = 0 \quad \text{Eq. 10}$$

(x,y) : stationary coordinate system

(u,v) : velocity in the stationary coordinate system

(X,Y) : rotational coordinate system

(U,V) : relative velocity

θ :rotational angular

ω : angular velocity ; $\omega t = \theta$

p : pressure

Re: Reynolds number

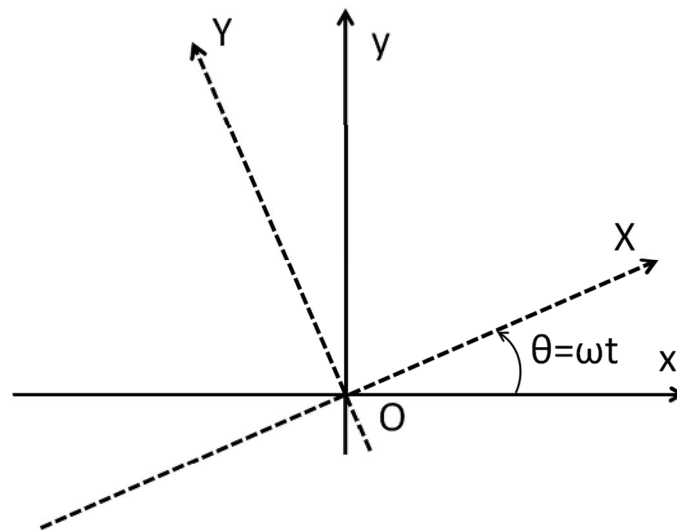


Fig. 3 The coordinate systems

The Fractional step method which can split the pressure term and the others are used. The pressure is derived from the Poisson equation. The linear spatial derivatives are approximated by the central differences. The third order upwind differences are used for the nonlinear derivatives. With this method, stable solutions are provided without any turbulence models.

Figure 4 shows the partial view of computational grid. In this figure, the lines are drawn every three to be shown clearly. This grid is made with using transfinite interpolation which can be applied for complex boundaries, that is one of the grid generation method. The number of grid points are 189×153 .

Initially, the boundary conditions on the blade are set to no-slip, and a far-field is uniform-flow velocity. The Reynolds number is fixed to 2000 based on the rotor diameter and uniform-flow velocity in this study.

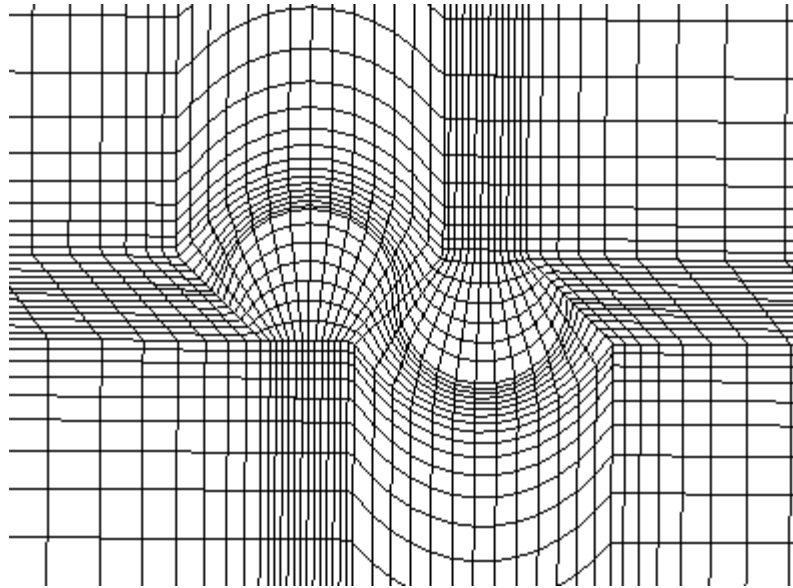


Fig. 4 The partial view of computational grid

3.Results and Discussions

The torque T of the rotor is calculated as the product of the force which applies to the blade and the distance from the center of the rotor. The torque coefficient C_t is calculated from the following equation(Eq.11). The power coefficient C_p means the energy which can extract from the wind(Eq.12).

$$C_t = \frac{T}{qRA} \quad \text{Eq. 11}$$

$$C_p = \lambda C_t \quad \text{Eq. 12}$$

C_t : torque coefficient

q : dynamic pressure

A : swept area

C_p : power coefficient

Figure 5 shows the torque coefficient variations of the rotor in a revolution at $\lambda=0.8$. Under the condition of the blade shape at $b=1.25$, the negative value region of C_t is reduced compared with others.

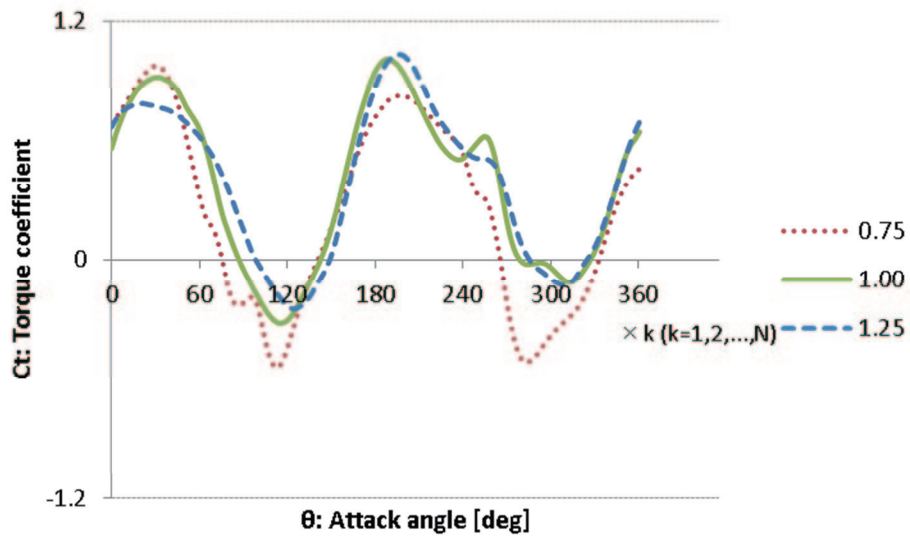


Fig. 5 The variation of torque coefficients($\lambda=0.8$)

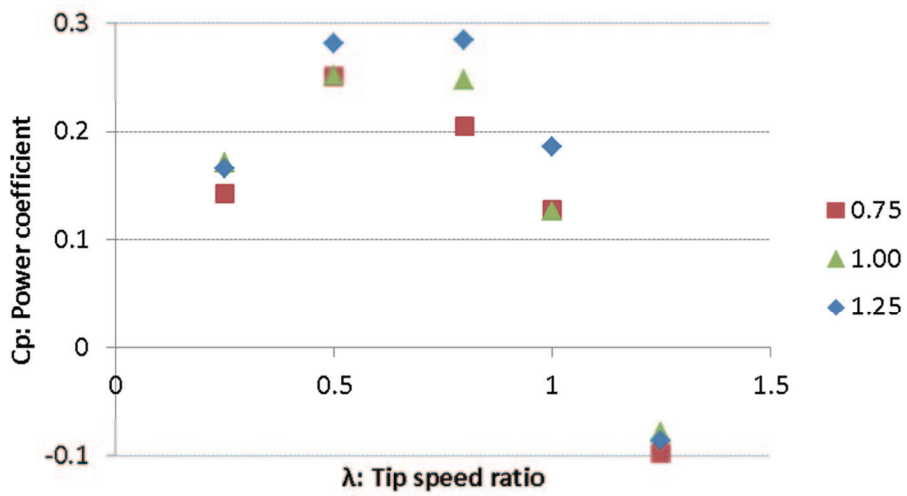


Fig. 6 The power coefficients of three types of blade

The power coefficients of various tip speed ratio are shown in Figure 6. This result is qualitatively in agreement with the experimental result.^[2] The blade shape of $b=1.25$ has the maximum power coefficient value of 0.28 at $\lambda=0.8$.

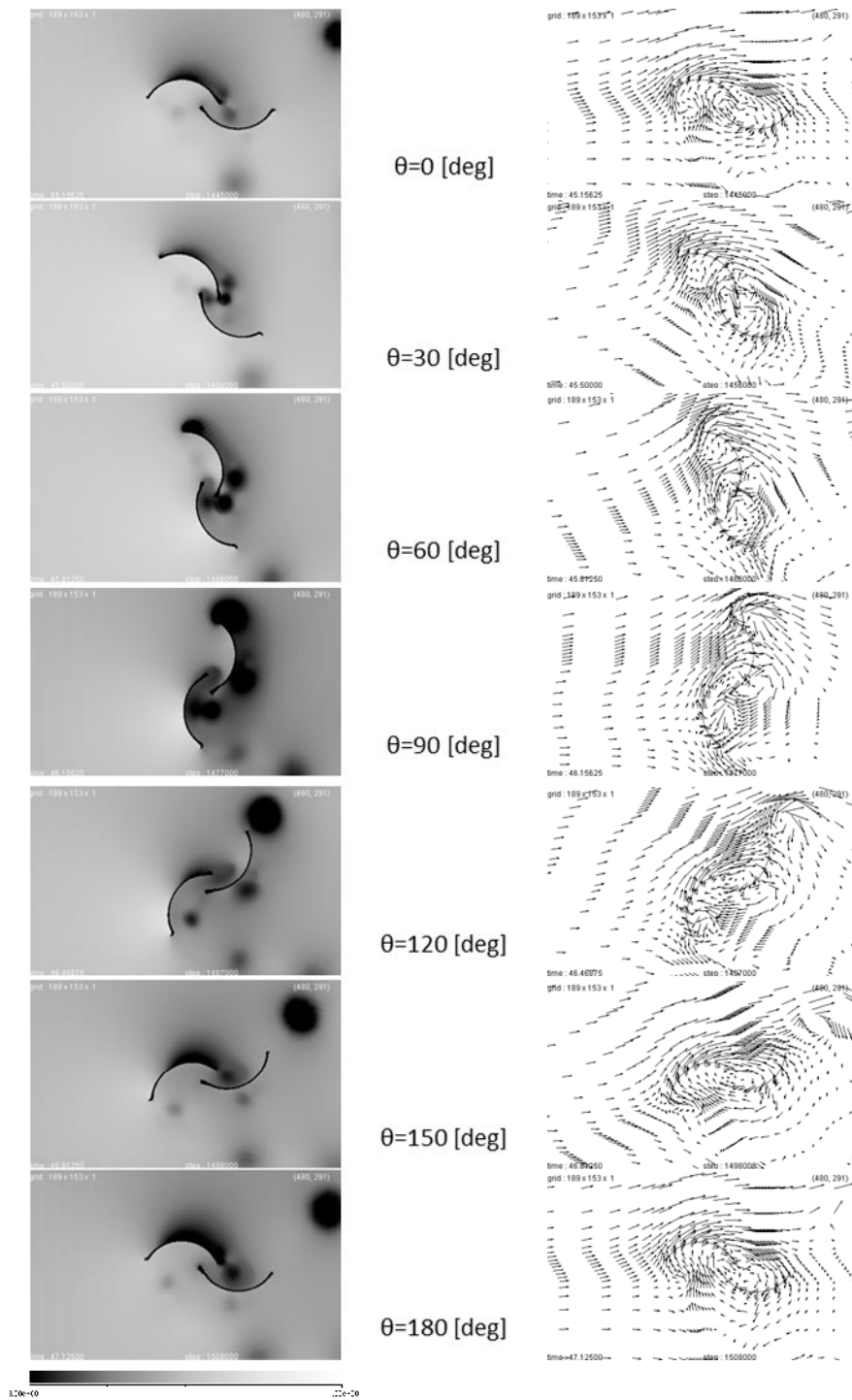


Fig. 7 The pressure contours and velocity fields ($b=0.75, \lambda=0.8$)

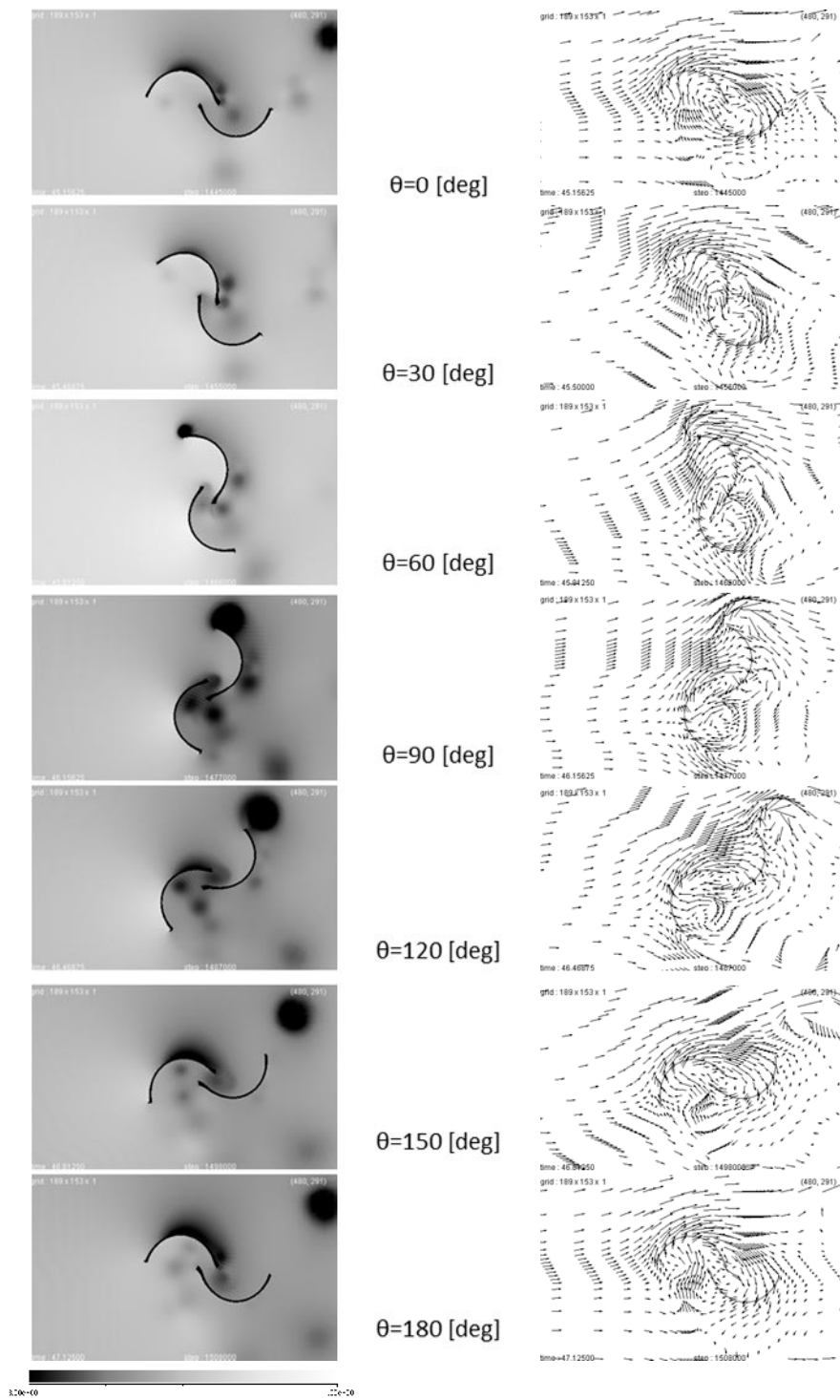


Fig. 8 The pressure contours and velocity fields ($b=1.00, \lambda=0.8$)

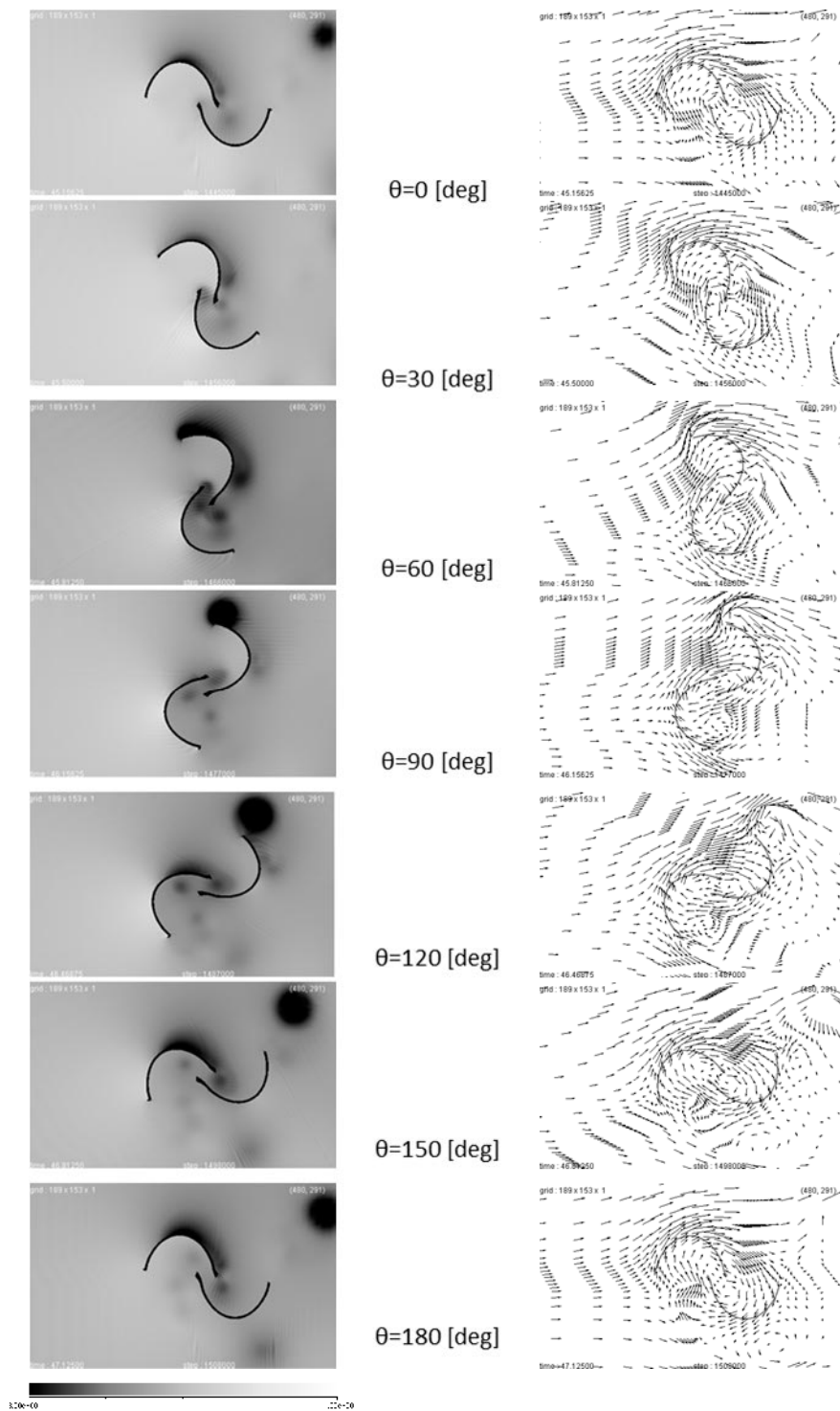
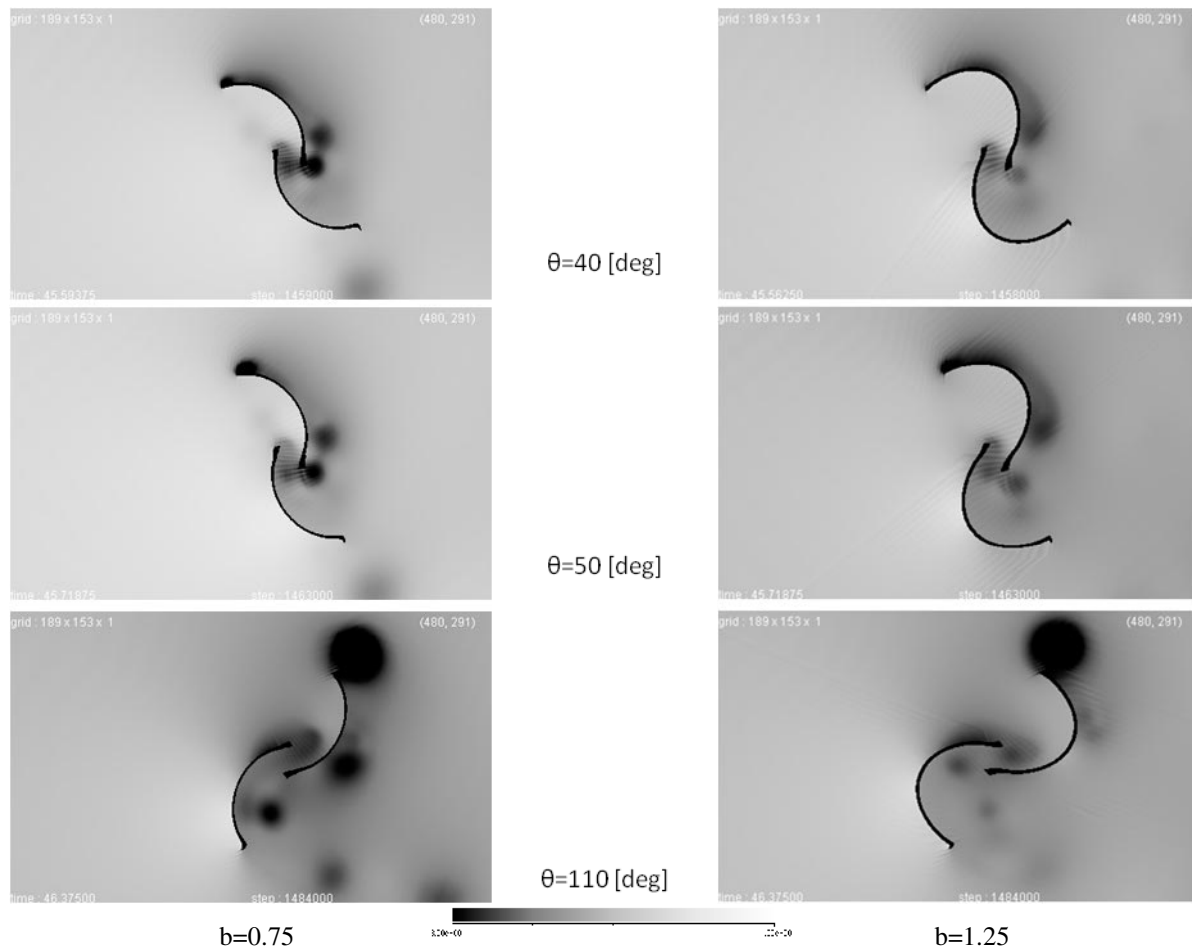


Fig. 9 The pressure contours and velocity fields ($b=1.25, \lambda=0.8$)

Figure 7 to 9 show the pressure contours and velocity fields of three types of blades at $\lambda=0.8$. The blade shape of $b=1.25$ has the maximum power coefficient value and the shape of $b=0.75$ had the minimum, and then these two types are compared in details as follows.



**Fig. 10 The pressure contours of $b=0.75$ and $b=1.25$
at $\theta = 40, 50, 110(+180 \times k ; k=0,1,2,\dots,N)$ [deg] ($\lambda = 0.8$)**

The blade shape of $b=0.75$, the vortex formation starts around $\theta=40(+180 \times k ; k=0,1,2,\dots,N)$ [deg] and released from tip of the blade around $\theta=110(+180 \times k ; k=0,1,2,\dots,N)$ [deg]. On the other hand, $b=1.25$, the vortex formation starts around $\theta=50(+180 \times k ; k=0,1,2,\dots,N)$ [deg] and released $\theta=110(+180 \times k ; k=0,1,2,\dots,N)$ [deg]. Furthermore, under the condition of $b=0.75$, other vortexes are formatted near the center of the rotor. For these reasons, the blade shape of $b=1.25$ has the maximum power coefficient and $b=0.75$ has the minimum.

4. Conclusions

The modified Savonius rotors are numerically investigated in this study. The results of the calculation qualitatively agrees well with the experimental data. In terms of the power coefficient, the condition of the blade shape at $b=0.75$ has the lower value and the shape at $b=1.25$ has the higher value compared with the conventional Savonius rotor. From the observation of the pressure fields, the vortex which forms on the tip of the blade is released earlier than others at the blade shape of $b=1.25$. For this reason, the blade shape of $b=1.25$ has the maximum power coefficient.

References

- [1] S.J.Savonius, The S-rotor and its application, *Mechanical Engineering*, 53(5), 333-338, 1931
- [2] Izumi Ushiyama, Hiroshi Nagai and Mashiro MINO, The OPTIMUM DESIGN CONFIGURATIONS OF SAVONIUS WIND TURBINES, *Proceedings of the Seventeenth Intersociety Energy Conversion Engineering Conference*, 4, 2096-2101, 1982
- [3] Nobuyuki Fujisawa, Velocity measurements and numerical calculations of flow fields in and around Savonius rotors, *Journal of Wind Engineering and Industrial Aerodynamics*, 59, 39-50, 1996
- [4] K.Ishimatsu, T.Shinohara and F.Takuma, Numerical simulation for Savonius rotors (running performance and flow fields), *JSME(B)*, 60(569), 154- 160, 1994
- [5] Anna Kuwana, Yuko Sato, Tetuya Kawamura, Numerical simulation for modified S-shaped wind turbines, *Kyoto University Research Information Repository*, 1539, 43-50, 2006
- [6] M.A. Kamoji, S.B. Kedare, S.V. Prabhu, Performancetests on helicalSavoniusrotors, *Renewable Energy*, 34(3), 521–529, 2009
- [7] Y.SATO, Y.YOSHIDA and T.KAWAMURA, *CFD Journal*, in press, 2011

Yuka yoshida

Otsuka 2-1-1, Bunkyo-ku, Tokyo 112-8610, Japan

Shin-Nakahara-Cho 1, Isogo-ku, Yokohama 235-8501, Japan

e-mail: yuka_yoshida@ihi.co.jp

Tetuya Kawamura

Otsuka 2-1-1, Bunkyo-ku, Tokyo 112-8610, Japan

e-mail: kawamura@is.ocha.ac.jp